COMPDYN 2013
4th ECCOMAS Thematic Conference on
Computational Methods in Structural Dynamics and Earthquake Engineering
M. Papadrakakis, V. Papadopoulos, V. Plevris (eds.)
Kos Island, Greece, 12–14 June 2013

ON THE EFFECT OF DAMPING ON DISPERSION CURVES IN PLATES

E. Manconi[1], **S. Sorokin**[2]

[1]Dipartimento di Ingegneria Industriale, Università degli Studi di Parma, Italy
e-mail: elisabetta.manconi@unipr.it

[2] Department of Mechanical and Manufacturing Engineering, University of Aalborg, Denmark
e-mail: svs@m-tech.aau.dk

Keywords: Guided waves, Damping, Viscoelasticity, Dispersion, Finite Element, Rayleigh-Lamb problem.

Abstract. *This paper presents a study on quantitative prediction and understanding of time-harmonic wave characteristics in damped plates. Material dissipation is modelled by using complex-valued velocities of free dilatation and shear waves in an unbounded volume. A Wave Finite Element (WFE) method is used to solve the Rayleigh-Lamb problem for a viscoelastic plate in plain strain, and results are validated using a Finite Product (FP) method. A numerical example concerning a viscoelastic panel is then presented in order to illustrate and discuss the role of dissipation in the cut-off phenomenon and in the phenomenon of veering for dispersion curves. These phenomena are explained in more detail considering a simple model, which allows accurate asymptotic analysis of the perturbation of dispersion curves in the regions of cut-off and veering.*

1 INTRODUCTION

The propagation of waves in plate-like structures has been the subject of a number of studies. Starting from the paper by Lamb in 1917 [1], a lot of effort has been devoted to the analytical, semi-analytical, and numerical prediction of dispersion curves and wave modes up to high frequency. Plates and shells are in fact part, or the main part, of many systems and understanding of guided wave propagation in such structures is fundamental in a number of applications, e.g. shock response, structure-born sound, acoustic emission etc. In particular, theoretical knowledge of dispersive behaviour up to high frequency is of importance in structural health monitoring (SHM) and non-destructive testing (NDT). As an example long-range and short-range ultrasonic guided waves are well established techniques for SHM and material characterisation, e.g. [2, 3]. Understanding of the behaviour of propagating waves modes is thus of direct relevance for better implementation of these techniques. However, many materials and panel constructions (such as metallic panels treated with viscoelastic layers or sandwich panels) show damping which can change the dispersive scenario and attenuate the wave signal, resulting in failure of results prediction and tests if the dissipation is not taken into account in the model.

Only recently the effect of material dissipation on wave propagation characteristics has received attention. The influence of material attenuation on Lamb wave dispersion behavior was investigated analytically in [4]. In this paper it was shown that when the degree of material attenuation is increased, dispersion curves for different modes of the same symmetry can cross instead of veering, which is the typical dispersive behaviour for an elastic plate. Simonetti and Lowe [5] studied shear horizontal wave propagation in elastic plates coated with viscoelastic materials showing the same scenario: compared to non-dissipative structures, real dispersion curve can cross instead of veering if the material attenuation is high enough. In [6] a prediction of energy velocity of attenuative guided waves in plates, together with an experimental validation of some results, was given. In [7] a spectral finite element method (SFEM) was used for modelling wave propagation in viscoleastic plates and evaluating energy velocity and waves attenuation. Comparison between results obtained for an hysteretic and a Kelvin-Voigt viscoelastic model of an orthotropic plate were also presented. In [7] it was also shown that the viscoleastic model has little effect on the phase and energy velocity. In [8] the SFEM was used for studying elastic guided waves in composite viscoelastic plates of different stacking sequences, while in [9, 10] a Wave Finite Element (WFE) method was applied for predicting wave dispersion, wave attenuation, and loss factor in viscoelastic laminated panels.

The aim of this paper is to present a study on quantitative prediction and understanding of wave propagation characteristics in damped plates up to high frequency. In particular Rayleigh-Lamb waves propagating in thick viscoleastic isotropic plate are investigated using an exact method, the Finite Product Method (FPM) [11, 12], and the Wave Finite Element (WFE) method [13, 14, 9]. Compared to other works on the same subject, dispersive behaviour is illustrated and discussed in the complex wavenumber plane and an illustrative example is given to explain and interpret some general features that spatially damped wave modes in plates have, or may have, in common. In the second section of the paper modelling of material losses in terms of complex-valued velocity is discussed. Material properties are obtained from these complex velocities in order to apply the WFE method. In Section 3 the FP method and the WFE method are briefly introduced and reviewed. Section 4 is devoted to numerical results. The propagation of guided waves in a thick viscoleastic plate are interpreted in terms of complex dispersion curves and the main effects of damping are illustrated. It is shown that material losses affect the dispersive behaviour in terms of cut-off frequencies and veering of wavemodes. These are

investigated in section V considering an illustrative model of coupled waveguides, similar to those presented in [15], which allows accurate asymptotic analysis.

2 WAVE PROPAGATION IN DAMPED PLATES.

In damped plates, solving the dispersion relation involves two cases:

a) the real-valued wavenumber and its direction are given and the (complex) frequencies are to be found, that is space-harmonic initial conditions are applied, spatial decay is prevented, and transient vibrations with decaying amplitudes are generated;

b) the real-valued frequency is given and the (complex) wavenumbers are to be found, that is the time-harmonic excitation is considered (time decay is prevented) but spatially attenuating waves are generated.

Thus, according to a) or b) waves are attenuated either in time or in space, respectively. In this work, case b) is considered, that is spatially damped time-harmonic waves are assumed throughout the paper. In particular, for this type of waves, we are concerned with the cut-off and the veering phenomena.

As soon as material losses are accounted for, all wavenumbers become complex-valued. Therefore, the concept of cut-off frequency needs a revision in this context. In a waveguide without damping, the cut-off frequency for a given branch of the dispersion diagram is found from the condition that the imaginary part Im[k] (k is the wavenumber) vanishes, which can occur either when Re[k]$= 0$ or when Re[k]$\neq 0$, where k is the wavenumber. In the 3D space (Ω, Re[k], Im[k]), this corresponds to the sharp turn of the branch onto the Im[k]$= 0$ plane. The presence of damping invalidates this simple definition. In what follows, we identify a cut-off frequency range as the frequency range at which the imaginary part of a wavenumber becomes sufficiently small and, more importantly, its decay rate diminishes and becomes to be "controlled" only by the damping coefficient. For small amounts of damping, the cut-off frequency range is centred at the cut-off frequency for a waveguide without material losses. Veering/mode repulsion is also strongly affected by the presence of material losses. Specifically, in the absence of damping, the veering of propagating waves occurs in the Im[k]$= 0$ plane, whereas in a plate with material losses dispersion curves can avoid intersection in a different manner, as illustrated in this paper.

2.1 Modelling of material losses: complex-valued velocity and material properties.

Modelling material dissipation is a crucial issue and it has been discussed in many studies, e.g. [16]. In modelling the energy dissipation due to viscosity of the material of a waveguide, we adopt the methodology outlined in [17], Vol. II, p. 315, for the linear time-harmonic acoustic waves. We use the complex-valued velocities $c_1 = c_{1r} + \mathrm{i}c_{1i}$ and $c_2 = c_{2r} + \mathrm{i}c_{2i}$ instead of the pure real-valued velocities of dilatation and shear waves. The Young's modulus and Poisson's ratio can thus be obtained as

$$E = \frac{\rho c_2^2 \left(3c_1^2 - 4c_2^2\right)}{\left(c_1^2 - c_2^2\right)}; \quad \nu = \frac{\left(c_1^2 - 2c_2^2\right)}{2\left(c_1^2 - c_2^2\right)}. \tag{1}$$

These may be constant or proportional to the frequency and temperature according to the type of damping the analyst is considering.

In what follows the viscoelastic model is used under the assumption that the complex-valued velocities of dilatation and shear waves are frequency independent. Although this is an idealised model, it allows a reasonable and quite general representation of properties of many dissipative materials.

3 The Rayleigh-Lamb problem

In this section the Rayleigh-Lamb problem is solved using a WFE method and FP method. The two methods are briefly described. We consider stationary time-harmonic free waves in an infinitely long straight layer of visco-elastic material with traction-free boundary conditions in plane strain state. The thickness of this layer is h.

3.1 The Wave Finite Element Method

The WFE method is a numerical technique which combines FE analysis and the theory of wave propagation in periodic structures. A detailed description of the method for flat and curved panels can be found in [13, 14] and, for sake of brevity, is not illustrated in details here. The WFE method is a systematic and straightforward approach which combines the theory of wave propagation in periodic structures with conventional FE analysis. As such, it is an application of FE analysis to periodic structures, although in the case considered in this paper the structure is homogeneous in the x and y directions, and hence the periodicity of arbitrary length. Compared to similar methods the WFE approach offers some advantages: (i) typically commercial FE packages can be used to generate the model, (ii) no new elements need to be derived and implemented - as in the the Spectral Finite Element method, (iii) it can be easily applied to 1D and 2D waveguides, and (iv) the computational cost is extremely small. In particular, as also described in [9], using different types of elements and increasing the number of elements meshed through the thickness is a trivial task. This enables the shear distribution to be correctly represented and the energy dissipation to be accurately evaluated, in particular in laminated plates with soft layers or when constrained layer damping treatments are applied. The method has been validated by a number of benchmark cases and it has been seen to provide accurate solutions at small computational cost. In particular viscoelasticity can be straightforwardly included in the WFE formulation in order to predict wave attenuation and the loss factor as shown in [9, 10].

Compared to the 2D formulation in [13], in this paper a 1D formulation (similar to those presented in [18]) is considered. In summary, a section of axial length L is taken from the structure and meshed using a stack of FE elements as indicated in Fig. 1. In this paper, for example, plane elements in plain strain are used, but solid elements or other types of elements can be used. The mass $\mathbf{M}$ and stiffness $\mathbf{K}$ matrices of the FE model are typically found using commercial FE packages. Damping can be included considering viscous matrix $\mathbf{C}$ or structural damping $\mathbf{K} = \mathbf{K}' + \mathrm{i}\mathbf{K}''$ as in this paper, [13, 9]. Therefore FE equation of motion of the section becomes

$$\mathbf{D}\mathbf{q} = \mathbf{f}, \tag{2}$$

where $\mathbf{D} = \mathbf{K} - \omega^2\mathbf{M}$ is the dynamic stiffness matrix of the segment, while $\mathbf{q}$ and $\mathbf{f}$ are the nodal degrees of freedom (DOFs) and nodal forces. The corner's DOFs and nodal forces are then concatenated into sets $\mathbf{q} = [\mathbf{q}_L^{\mathrm{T}}, \mathbf{q}_R^{\mathrm{T}}]^{\mathrm{T}}$ and $\mathbf{f} = [\mathbf{f}_L^{\mathrm{T}}, \mathbf{f}_R^{\mathrm{T}}]^{\mathrm{T}}$ associated with the left L and the right R sides of the segment as shown in Fig. 1, and the FE equations of motion is partitioned into

$$\begin{bmatrix} \mathbf{D}_{LL} & \mathbf{D}_{LR} \\ \mathbf{D}_{RL} & \mathbf{D}_{RR} \end{bmatrix} \begin{bmatrix} \mathbf{q}_L \\ \mathbf{q}_R \end{bmatrix} = \begin{bmatrix} \mathbf{f}_L \\ \mathbf{f}_R \end{bmatrix}. \tag{3}$$

Consider a plane wave propagating in the waveguide according to

$$w(x, y) = We^{\mathrm{i}(-kx+\omega t)}, \tag{4}$$

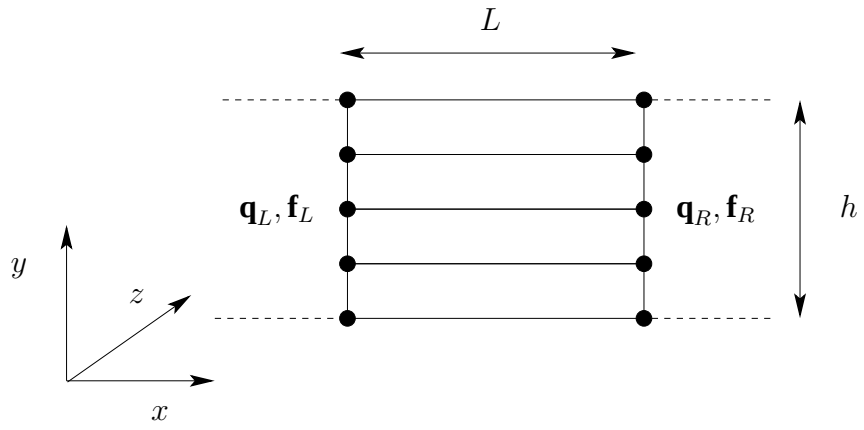

Figure 1: FE model of a section of the waveguide.

where $W(y)$ is the wave mode, ω is the angular frequency and k is the wavenumber. Under the passage of the wave, the nodal DOFs are related by periodicity conditions, [19],

$$\mathbf{q}_R = \lambda \mathbf{q}_L, \tag{5}$$

where $\lambda = e^{-\mathrm{i}kL}$, while equilibrium at the left side of the segment implies

$$[\mathbf{I} \quad \lambda^{-1}\mathbf{I}]\mathbf{f} = \mathbf{0}. \tag{6}$$

The equation of motion of the segment is projected onto the DOFs $\mathbf{q}_L$ using Eqs. (5) and (6), providing a WFE reduced eigenvalue problem whose solutions yield the dispersion curves and the wave mode shapes. For spatially damped waves the real-valued frequency is given and the (complex) wavenumbers are to be found. This involves solving the quadratic polynomial eigenvalue problem in λ

$$[\mathbf{D}_{LR}(\omega)\lambda^2 + (\mathbf{D}_{LL}(\omega) + \mathbf{D}_{RR}(\omega))\lambda + \mathbf{D}_{RL}(\omega)]\mathbf{q}_L = \mathbf{0}, \tag{7}$$

which can be recast as a standard linear eigenvalue problem. Once dispersion curves and wave-modes are obtained, a number of other quantities can be evaluated. For example the forced response can be found straightforwardly, [20, 21].

3.2 Exact Formulation and the Finite Product Method

The standard Lamé decomposition of the displacement field $\mathbf{u} = (u_x, u_y, o)^T$ is employed

$$\mathbf{u} = \nabla \cdot \Phi + \nabla \times \mathbf{i}_z \Psi, \tag{8}$$

where Φ and Ψ are scalar potentials, while $\mathbf{i}_z$ is the unit vector. The potentials Φ and Ψ are governed by the Helmholtz equations (c_1 and c_2 are velocities of dilatation and shear waves, respectively):

$$\nabla^2\Phi + \frac{\omega^2}{c_1^2}\Phi = 0; \quad \nabla^2\Psi + \frac{\omega^2}{c_2^2}\Psi = 0. \tag{9}$$

Due to the symmetry in the boundary conditions at $y = \pm h/2$, the symmetric and skew-symmetric modes are considered independently from each other, and the dispersion equations are:

$$\frac{\tan(q/2)}{\tan(p/2)} = -\frac{4k^2pq}{(q^2-k^2)^2} \tag{10}$$

for symmetric modes, and

$$\frac{\tan(q/2)}{\tan(p/2)} = -\frac{(q^2-k^2)^2}{4k^2pq} \tag{11}$$

for skew-symmetric modes, where $p^2 = \left(\frac{\omega h}{c_1}\right)^2 - k^2$, $q^2 = \left(\frac{\omega h}{c_2}\right)^2 - k^2$. These dispersion equations may be solved by various methods.

In what follows, we apply the FP method. This method was proposed very recently [11, 12], and its fundamental advantage is the absence of spurious roots. The key idea in the FP method for a planar layer is to start with the exact dispersion relations of Rayleigh-Lamb theory, and replace the sine and cosine terms by finite-product polynomials, chosen to have the same roots as the original sines and cosines in a finite region. After this step has been taken, all calculations are performed with polynomials, and the original transcendental dispersion relation is not used again, unless accuracy analysis is required. The dispersion equations are rewritten as follows:

$$L_3^4 S_2 C_1 + K^2 L_1^2 C_2 S_1 = 0 \tag{12}$$

for symmetric modes, and

$$L_3^4 S_1 C_2 + K^2 L_2^2 C_1 S_2 = 0 \tag{13}$$

for skew-symmetric modes. Here $S_i = S(L_i^2/4)$, $C_i = C(L_i^2/4)$, $L_i^2 = \Omega_i^2 - K^2$, $i = 1, 2$ and $L_3^2 = \frac{1}{2}\Omega_2^2 - K^2$, where Ω is the angular frequency. Furthermore, $(K, \Omega_1, \Omega_2) = (kh, \omega h/c_1, \omega h/c_2)$. The functions S and C are defined by $S(s^2) = s^{-1}\sin(s)$ and $C(s^2) = \cos(s)$. The use of S and C, rather than sine and cosine, helps avoid square roots in equations, where the square roots ultimately cancel out in pairs, and so maintains a polynomial form. The finite products are defined as follows:

$$S_{mi} = \prod_{m'=1}^{m}\left(1 - \frac{L_i^2}{4(m'\pi)^2}\right); \quad C_{ni} = \prod_{n'=1}^{n}\left(1 - \frac{L_i^2}{(2n-1)^2\pi)^2}\right); \quad i = 1, 2. \tag{14}$$

If $m = 0$ or $n = 0$, the value of the corresponding finite product is defined as 1. Then the Eqs. (13,12) are approximated by:

$$L_3^4 S_{m2} C_{n1} + K^2 L_1^2 C_{n2} S_{m1} = 0; \quad L_3^4 S_{m1} C_{n2} + K^2 L_2^2 C_{n1} S_{m2} = 0. \tag{15}$$

The dispersion curves presented in the next section (as the reference solution) are obtained by means of the FP method with $m = 13$ and $n = 14$. At this level of approximation, the finite-product results are virtually undistinguishable from the results obtained solving the original transcendental dispersion equations in the considered (k, Ω) windows, while, at the same time, the computational effort to obtain the dispersion diagrams is profoundly less. The polynomial approximations in fact introduce no spurious branches into the dispersion relation, and are ideal for numerical computation. The FP polynomial approximation of dispersion equations is potentially useful for a very wide range of problems in wave theory and stability theory and it is particularly advantageous for calculations of the complex-valued roots.

4 Numerical results and discussion.

In this section numerical results are presented for a $h = 6$ mm thick viscoleastic isotropic plate. The material considered in this numerical example is a high performance polyethylene. Material properties are taken from [6]. In particular it is assumed that complex wave velocity are: $c_1 = 2346.6 - \mathrm{i}99.54$ m s^{-1}, $c_2 = 951 - \mathrm{i}40.31$ m s^{-1}. Material density is $\rho = 953$ kg m^{-3}.

In this example, the WFE model is realized using 150 plane elements (in plane strain) of the type PLANE42 in Ansys. These elements are meshed through the cross sections, see Fig. 1. The length of the element in the x direction is $L = 0.5$ mm. The same value is assumed for the thickness of the element in the y direction. The real valued dispersion curves, which represent propagating waves for the undamped plate and the corresponding real parts of complex wave numbers for the damped plate, are given in Fig. 2(a), while Fig. 2(b) shows the corresponding wave attenuation in the damped plate - notice that the imaginary part of wavenumbers for propagating waves in an undamped plate is zero. Comparison with results obtained using the FP method has shown excellent agreement - dispersion curves obtained using the WFE method and the FP method are indistinguishable. In Fig. 2, for the sake of clarity, only spatially damped waves which propagate in the absence of damping are plotted. Highly attenuated waves with large imaginary parts of wavenumbers are not shown.

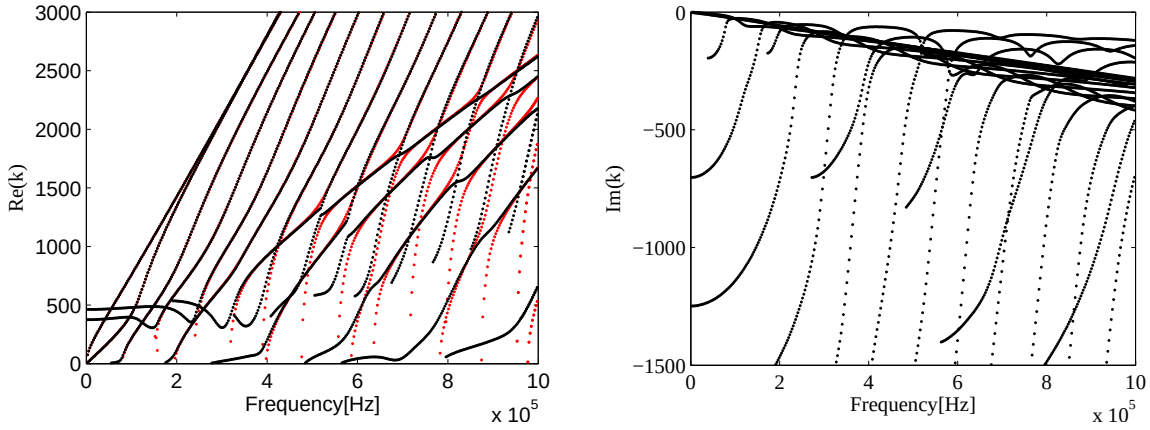

Figure 2: (a) Real valued dispersion curves for the undamped and damped plate; (b) waves attenuation for the damped plate. Black lines: damped case; red lines: undamped case.

Fig. 2 shows that the dispersion curves for the undamped and damped panels differ mainly in terms of cut-off frequencies and veering. The cut-off phenomenon in the complex wavenumber space is illustrated in Fig. 3. Dispersion curves follow two different scenarios for cut-off, which in the absence of damping are: i) dispersion branches cut-off when Re(k)$\neq 0$ but Im(k)$= 0$; ii) dispersion branches cut-off when Re(k)$= 0$ and Im(k)$= 0$. Case i) for the damped plate is shown in Fig. 3(b), (branch 1 and 2). For the sake of clarity only symmetric wave modes are plotted. In the figure negative and positive values of both the real and imaginary part of wavenumbers are plotted in order to highlight some important details of interaction between the branches. Sufficiently far from the "transition zone", branch 1 (plate with damping) is located close to the branch for plate with no damping. In the absence of damping, it can be seen that, as the frequency increases, firstly two complex branches transform into two pure real branches (branches 3 and 4). Then these branches sharply become pure imaginary (branches 5 and 6) and then they transform again into pure real branches (branches 7 and 8). Due to the presence of damping these transitions from pure real to pure imaginary wavenumbers are smoothened, and the damped branches spiral around each other acquiring different imaginary part of the wavenumber (branch 1 and 2). As the frequency grows, branch 1 tends to branch 7. Case ii) is shown in Fig. 3(c). For the sake of clarity only symmetric wave modes are plotted. In the absence of damping, two complex valued branches (branches 10 and 11) become purely imaginary. One of them (branch 12) turns to become two pure real branches (branch

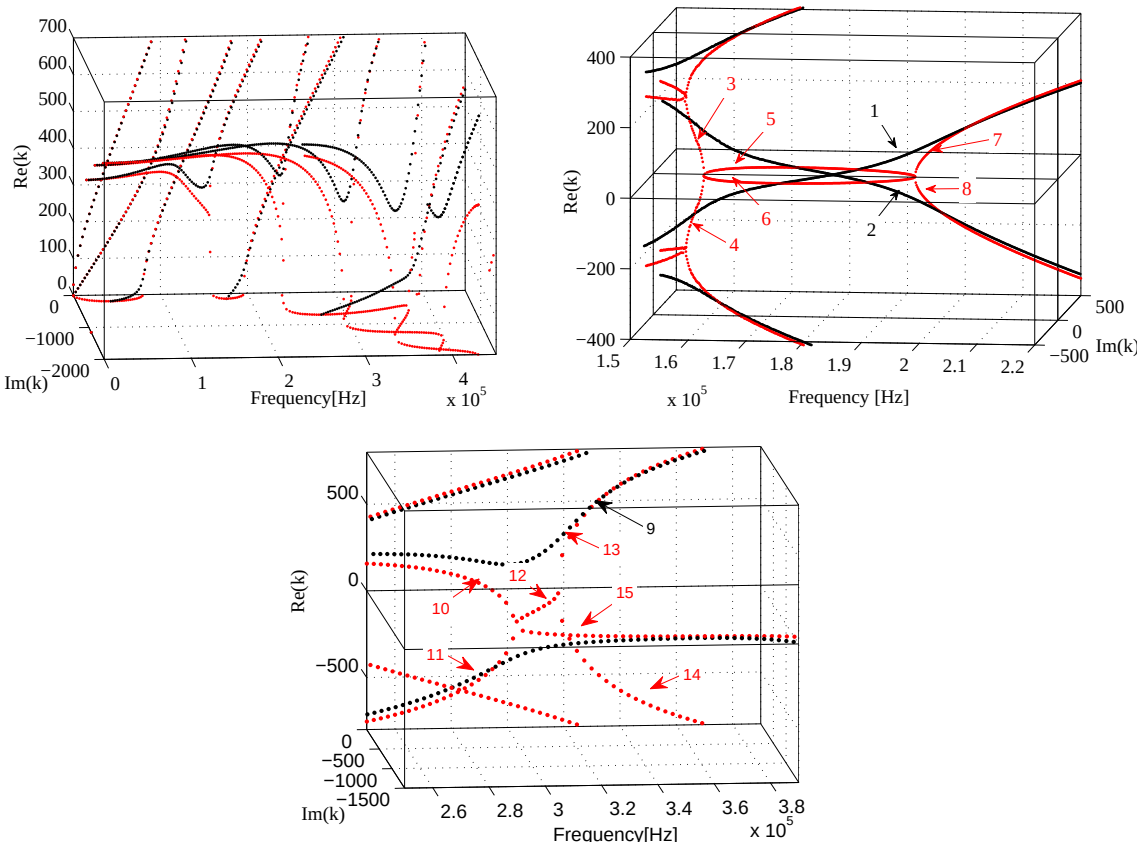

Figure 3: (a) Dispersion curves in the complex wavenumber space; (b) case i) - dispersion curves close to a cut-off frequency; (c) case ii) - dispersion curves (only symmetric waves) close to a cut-off frequency. Black lines: damped case; red lines: undamped case.

13 and branch 14) while the other (branch 15) remains in the imaginary plane until it becomes complex acquiring different signs of the real parts (branches 15 and 16). Again, the presence of damping smoothen the passage between pure real and pure imaginary wavenumbers: as the frequency increases the real and imaginary part of the wavenumber decay up to the real part reaches a minimum in the vicinity of the cut-off frequency of the undamped plate, then the real part grows while the imaginary part stabilises. This phenomenon can readily be captured and quantified in the solution of a simple model problem considered in the next section. In the case of an undamped plate, veering of two branches of the dispersion curves occurs, as seen in Fig. 2(a) and Fig. 4(a). This phenomenon is associated with an exchange of wavemode shapes between these two branches [15]. However, when dissipation is taken into account, curves presenting the frequency dependence of the real parts cross each other instead of veering, as seen in these figures. This behaviour has been noticed by other authors, e.g. [7]. Inspection into spatial location of dispersion curves in the (Ω, Re(k), Im(k)) space reveals that veering still takes place for damped wavemodes, but it occurs in a different manner. This is shown in Fig. 4(b) where dispersion curves are plotted in the complex space in a region close to the frequency around which veering occurs. This phenomenon can readily be captured and quantified in the solution of a simple model problem considered in the next section.

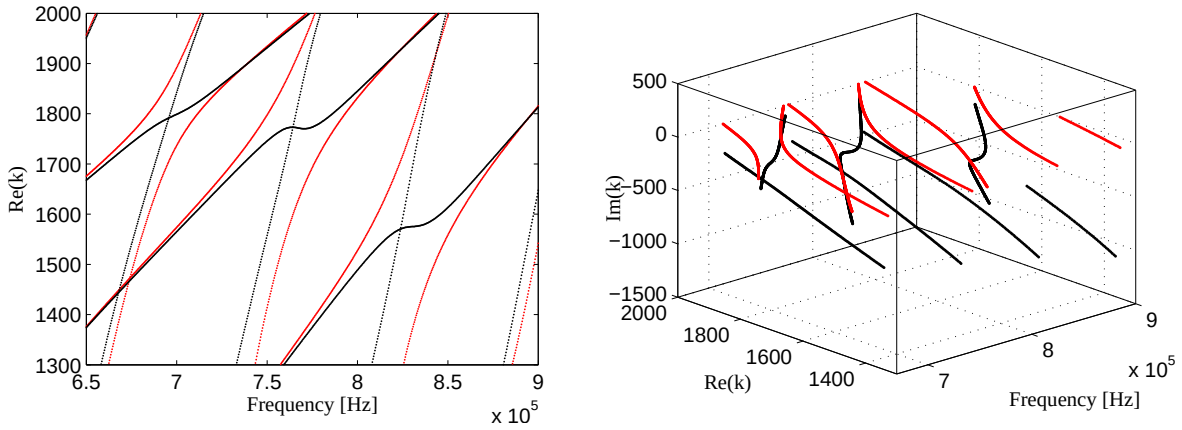

Figure 4: (a) Dispersion curves in a region close to coupling; (b) 3D plot of the complex dispersion curves in a region close to coupling. Black lines: damped case; red lines: undamped case.

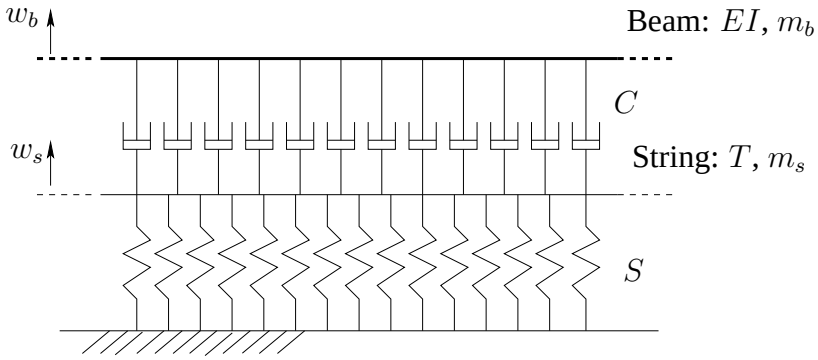

Figure 5: Illustrative example: coupled system.

5 ILLUSTRATIVE EXAMPLE

As it has been shown in the previous section, the material losses change the dispersive scenario. Once the losses are taken into account, the branches of dispersion curves avoid intersection by acquiring different imaginary parts. By these means, the real parts of wave numbers are allowed to be identical, which is impossible for waveguides with no energy dissipation. The presence of damping also features disappearance of cut-off frequencies, since all waves are attenuated at purely real-valued frequencies. These phenomena may be quantified and better understood in the analysis of the wave propagation using the model waveguide similar to the one considered in [15] shown and investigated in the next sections.

5.1 The model waveguide

The model considered in this section consists of a string (membrane) and a beam (plate) coupled as shown in Fig. 5. This is almost the simplest model which allows us to illustrate the veering and cut-off phenomena reported in the previous section. The string is exposed to tension T, it has a mass per unit length m_s and it rests on a Winkler elastic foundation of stiffness S. The beam is characterized by its bending stiffness EI and its mass per unit length m_b. The string is coupled with the beam via locally reacting uniformly distributed dashpot elements with damping coefficient C. The differential equations of motion of this system with respect to

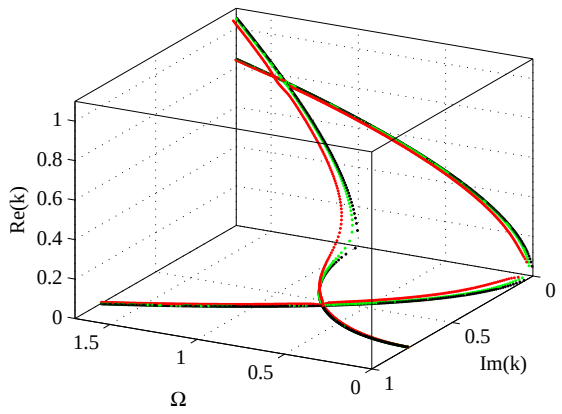

Figure 6: Illustrative example. Dispersion curves. Black lines: $\varepsilon = 0$; green lines: $\varepsilon = 0.01$; red lines: $\varepsilon = 0.05$.

the displacements w_b and w_s are:

$$\begin{gathered} EI\frac{\partial^4 w_b}{\partial x^4} + m_b\frac{\partial^2 w_b}{\partial t^2} + C\left(\frac{\partial w_b}{\partial t} - \frac{\partial w_s}{\partial t}\right) = 0; \\ -T\frac{\partial^2 w_s}{\partial x^2} + Sw_s + m_s\frac{\partial^2 w_s}{\partial t^2} - C\left(\frac{\partial w_b}{\partial t} - \frac{\partial w_s}{\partial t}\right) = 0. \end{gathered} \tag{16}$$

This simple model allows accurate analysis of the perturbations in the location of dispersion curves produced by the purely dissipative coupling elements. Where appropriate, the results of this analysis will be compared with the results obtained for a non-dissipative waveguide, in which spring elements are used instead of dashpots. Solution is sought as $w_b = W_b \exp(\mathrm{i}kx - \mathrm{i}\omega t)$, $w_s = W_s \exp(\mathrm{i}kx - \mathrm{i}\omega t)$. It is convenient to introduce the non-dimensional parameters and write the equations of free propagation of time-harmonic waves as:

$$\begin{gathered} \left(\alpha k^4 - \mathrm{i}\varepsilon\Omega - \delta\Omega^2\right) W_b + \mathrm{i}\varepsilon\Omega W_s = 0; \\ \mathrm{i}\varepsilon\Omega W_s + \left(\beta k^2 + 1 - \mathrm{i}\varepsilon\Omega - \Omega^2\right) W_b = 0. \end{gathered} \tag{17}$$

The notations are: $\Omega^2 = \dfrac{m_s\omega^2}{S}$, $k = k_{dim} r_g$, $\alpha = \dfrac{EI}{Sr_g^2}$, $\beta = \dfrac{T}{Sr_g^2}$, $\delta = \dfrac{m_g}{m_s}$, $\varepsilon = \dfrac{C}{\sqrt{Sm_s}}$, where r_g is the characteristic length scale, say, the gyration radius of the cross-section of a beam. The coupling parameter ε is small, so that classical perturbation methods may be used for the asymptotic analysis. Equating to zero the determinant of the system in Eq. (17) yields the dispersion equation, which is the polynomial of the third order in k^2. It is convenient to introduce the modal coefficient for each wave number, which satisfies the dispersion equation:

$$M = \frac{W_b}{W_s} = -\frac{\alpha k^4 - \mathrm{i}\varepsilon\Omega - \delta\Omega^2}{\mathrm{i}\varepsilon\Omega} = -\frac{\mathrm{i}\varepsilon\Omega}{\beta k^2 + 1 - \mathrm{i}\varepsilon\Omega - \Omega^2}. \tag{18}$$

Since the dispersion equation has the polynomial form, the method of dominant balance as described in [22] is perfectly suitable to find asymptotic formulas for its roots in various regions.

The dispersion diagrams for this waveguide are shown in Fig. 6. The parameters are chosen as $\alpha = 4$, $\beta = 1.4$, $\delta = 0.7$. Black curves are plotted for $\varepsilon = 0$, i.e. in the case of no coupling between a string and a beam. Green curves are plotted for the light damping, $\varepsilon = 0.01$, and red curves are plotted for $\varepsilon = 0.05$. We are interested in the asymptotic analysis of the influence of damping on the location of dispersion curves in the low-frequency $(\Omega \to 0)$ and the cut-off

$(k \to 0)$ limit cases, as well as in the veering zone, not displayed in this diagram. In each case, it is possible to obtain explicit formulas for the wave numbers to the leading order and explore the roles of parameters involved in the problem formulation.

5.2 The cut-off frequencies

The exact dispersion equation for $\varepsilon = 0$ is factorised to yield $k^4 = \frac{\delta\Omega^2}{\alpha}$ (the four branches of dispersion curves for the beam) and $k^2 = \frac{\Omega^2 - 1}{\beta}$ (the two branches of dispersion curves for a string). The asymptotic formulas for the perturbed wave numbers to the leading order are $k^4 = \frac{\delta\Omega^2}{\alpha} + \frac{\mathrm{i}\varepsilon\Omega}{\alpha}$ and $k^2 = \frac{\Omega^2 + \mathrm{i}\varepsilon\Omega - 1}{\beta}$. As seen, the leading order correction to the flexural wave numbers does not contain parameters of the membrane, and, likewise, the leading order correction to the axial wave numbers is independent on the parameters of plate. In the absence of damping, the cut-off frequencies, obviously, are $\Omega^{fl}_{cut-off} = 0$ and $\Omega^{axial}_{cut-off} = 1$. The dispersion diagrams in Fig. 7 are plotted in vicinity of these frequencies for the same three cases as in Fig. 6.

The purely real non-zero cut-off frequencies do not exist for a waveguide with damping, because all wave numbers are complex-valued at any real-valued frequency. In such a waveguide, the wave highly attenuated below cut-off frequency becomes lightly attenuated (only due to the presence of damping) as the frequency exceeds the cut-off value obtained when the damping is set to zero. This aspect was also shown in [5]. In contrast with the model of weak coupling of a string and a beam via distributed spring elements [15], the cut-off frequency for the flexural wave number equals zero. However, its low-frequency (for the fixed damping coefficient) asymptotic behaviour features $k \sim \Omega^{1/4}$, rather than $k \sim \Omega^{1/2}$. This difference is clearly seen in Fig. 7(a). The complex-valued wavenumber for a system with damping departs from the plane Im[k]$= 0$ and it asymptotically tends to this plane as frequency grows. This behaviour differs from the behaviour of dispersion curves for a viscoelastic layer in the vicinity of $\Omega = 0$. When

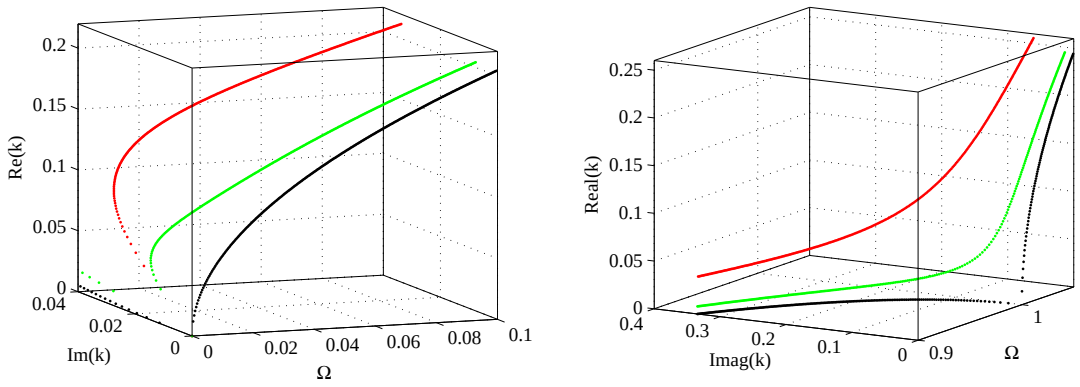

Figure 7: Illustrative example. (a) dispersion diagrams in the vicinity of $\Omega^{fl}_{cut-off} = 0$; (b) dispersion diagrams in the vicinity of $\Omega^{axial}_{cut-off} = 1$. Black lines: $\varepsilon = 0$; green lines: $\varepsilon = 0.01$; red lines: $\varepsilon = 0.05$.

$\varepsilon \neq 0$, it is convenient to determine the wave number of the dominantly axial wave at $\Omega = 1$, i.e. to find how much the dispersion curve is "repelled" from the point $(1, 0, 0)$ in the space of the dispersion diagram. To the leading order, this wave number is given by the formula $k = \sqrt{\frac{\mathrm{i}\varepsilon}{\beta}}$. Comparison of Fig. 3 and Fig. 7(b) shows that the simple model captures the behaviour of

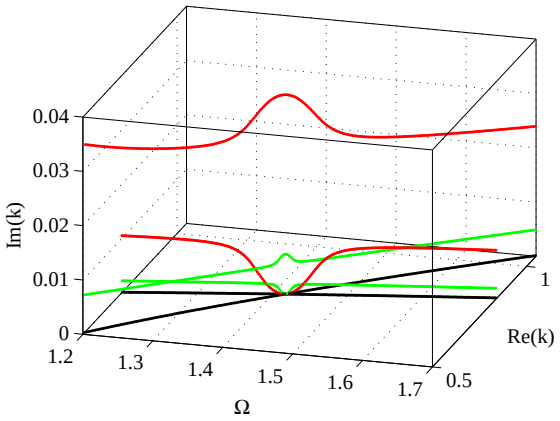

Figure 8: Illustrative example. Dispersion curves. Black lines: $\varepsilon = 0$; green lines: $\varepsilon = 0.01$; red lines: $\varepsilon = 0.05$.

dispersion curve for a viscoelastic layer near the plane Im[k]$= 0$.

5.3 The veering effect

In the case, when $\varepsilon = 0$, dispersion curves cross each other at the "coincidence" frequency $\Omega_c = \sqrt{1 + \frac{\delta\beta^2}{2\alpha} + \frac{\beta\sqrt{4\delta\alpha + \delta^2\beta^2}}{2\alpha}}$. The repeated wave number is $k_c^2 = \frac{\delta\beta}{2\alpha} + \frac{\sqrt{4\delta\alpha + \delta^2\beta^2}}{2\alpha}$. Obviously, the magnitudes of these frequencies and wavenumbers are dependent on all parameters of the waveguide. The dominant balance in the dispersion equation is obtained with the scaling: $\Omega = \Omega_c + \widehat{\Omega}\varepsilon$, $k^2 = k_c^2 + K_2\varepsilon$, $\widehat{\Omega} \sim O(1)$, $K_2 \sim O(1)$. The coefficients $\widehat{\Omega}$ and K_2 have been found in closed analytical form by means of the symbolic manipulator Mathematica 8.0. Dispersion curves shown in Fig. 8 are plotted in the veering zone for the same parameters as in Figs. 6-7. It can be noticed that, compared to the crossing in the (Ω,Re[k]) plane of dispersion curves in the uncoupled waveguide, here the dispersion curves are "repelled" from each other in the direction of Im(k) at the crossing point. This is opposite to the veering in the (Ω,Re[k]) plane which occurs in a waveguide with spring-type coupling elements, see [15].

The dispersion diagram plotted after the asymptotic formulas is compared with the results of direct numerical solution for $\varepsilon = 0.05$. Graphs in Fig. 9 show that these formulas are very accurate in the veering zone. As also seen in Fig. 9, at the "coincidence" frequency, one of the waves becomes purely propagating, whereas its counterpart is more heavily damped, than at other frequencies in the considered range. This effect has a simple physical explanation, which follows from the inspection in the frequency dependence of the modal coefficient shown in Fig. 10. This is the modal coefficient of the wave with the purely real wave number at $\Omega = \Omega_c$. At this frequency, the amplitudes of displacements (and velocities) of both components of the waveguide are the same and they move in phase. It means that the dashpot elements are not activated and the energy is conserved in this wave motion.

5.4 Relevance of the model problem

In a layer of the viscoelastic material considered in the previous section, viscosity influences cut-off frequency and produces veering effect similarly to what seen in the dispersion diagrams in Figs. 3. However, neither magnitude of the imaginary parts of the wave numbers involved in the veering vanishes at $\Omega = \Omega_c$, because each individual mode has its own losses. It is also problematic to identify the sub-waveguides interacting in the visco-elastic layer due to the

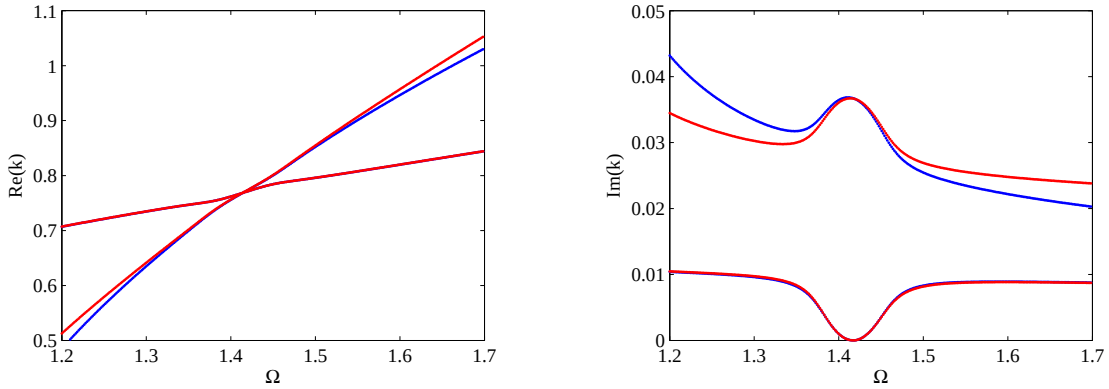

Figure 9: Illustrative example. Dispersion curves in the real and imaginary wavenumber plane, $\varepsilon = 0.05$. Blue lines: numerical solution; red lines: asymptotic solution.

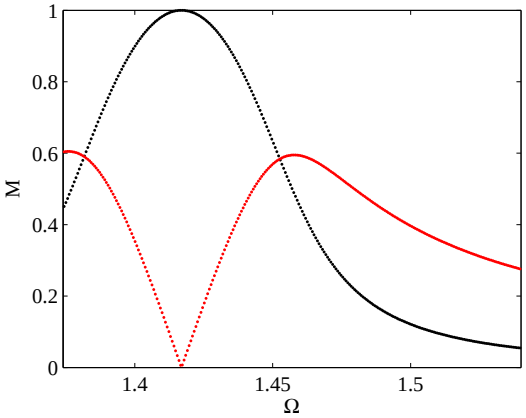

Figure 10: Illustrative example. Modal coefficient. Black lines: Re(M); red lines: Im(M).

energy dissipation as well as the damping coefficient for their coupling. Therefore, the model considered here serves for the qualitative analysis of the damping effects in the waveguides, in particular, in the viscoelastic layer.

6 Conclusion

A study on quantitative prediction and understanding of waveguide properties of viscoelastic plates is presented. A Wave Finite Element (WFE) method is used to solve the Rayleigh-Lamb problem for a viscoelastic plate, and results are validated using a Finite Product (FP) method, with the excellent agreement between these two. It is shown that the material losses affect the location of dispersion curves mainly in the cut-off and veering zones. Two cut-off scenarios in the absence and the presence of damping are identified and compared. In each case, it is shown that the dispersion curves for a plate with damping smoothly follow their counterparts for an undamped plate in 3D space (Ω, Re[k], Im[k]), avoiding sharp turns onto and out of the Im[k]$= 0$ plane. The veering scenarios are also investigated. For damped waves, the curves presenting real parts of complex-valued wavenumbers cross instead of veering (as it occurs for an undamped plate). However, dispersion branches avoid intersection by acquiring different imaginary parts of wavenumbers. An illustrative model of coupled waveguides is also investigated using asymptotic analysis in order to explain and interpret some general characteristics

that spatially damped wave modes have, or may have, in common.

REFERENCES

[1] H. Lamb, On waves in an elastic plate. *Proceedings of the Royal Society of London. Series A*, **93**, 114-128, 1917.

[2] D. E. Chimenti, Guided waves in plates and their use in materials characterization. *Applied Mechanics Reviews*, **50**, 247-284,1997.

[3] P. Wilcox and M. Lowe and P. Cawley, Lamb and SH wave transducer arrays for the inspection of large areas of thick plates. *in D.O Thompson, D.E Chimenti (Eds.), Annual review of progress in quantitative NDE*, **19**, 1049-1056, 2000.

[4] C. W. Chan and P. Cawley, Lamb waves in highly attenuative plastic plates. *Journal of the Acoustical Socitey of America*, **104**, 874-881, 1998.

[5] F. Simonetti and M. Lowe, On the meaning of Lamb mode non-propagating branches. *Journal of the Acoustical Socitey of America*, **118**, 186-192, 2005.

[6] A. Bernard and M. J. S Lowe and M. Deschamps, Guided waves energy velocity in absorbing and non-absorbing plates. *Journal of the Acoustical Socitey of America*, **110**, 186-192, 2001.

[7] I. Bartoli, A. Marzani, F. Lanza di Scalea, E. Viola, Modeling wave propagation in damped waveguides of arbitrary cross-section, *Journal of Sound and Vibration*, **2006**, 685-707, 2006.

[8] L. Taupin, A. Lheémery, G. Inquiété, A detailed study of guided wave propagation in a viscoelastic multilayered anisotropic plate. *Journal of Physics: Conference Series* **269**, 2011.

[9] E. Manconi and B. R. Mace, Estimation of the loss factor of viscoelastic laminated panels from finite element analysis. *Journal of Sound and Vibration*, **329**, 3928-3939, 2010.

[10] E. Manconi, B. R. Mace, R. Garziera, The loss-factor of pre-stressed laminated curved panels and cylinders using a Wave and Finite Element method. *Journal of Sound and Vibration*, **332**, 2013.

[11] C. J. Chapman, S. V. Sorokin, The finite-product method in the theory of waves and stability. *Proceedings of the Royal Society of London. Series A*, **466**, 471-491, 2010.

[12] S. V. Sorokin, C. J. Chapman, 2010. A hierarchy of rational timoshenko dispersion relations. *Journal of Sound and Vibration*, **330**, 5460-5473, 2011.

[13] B. R. Mace, E. Manconi, Modelling wave propagation in two-dimensional structures using finite element analysis. *Journal of Sound and Vibration*, **318**, 884-902, 2008.

[14] E. Manconi, B. R. Mace, Wave characterization of cylindrical and curved panels using a finite element method. *Journal of the Acoustical Socitey of America*, **125**, 154-163, 2009.

[15] B. R. Mace, E. Manconi, Wave motion and dispersion phenomena: veering, locking and strong coupling effects. *Journal of the Acoustical Socitey of America*, **131**, 1015–1028, 2012.

[16] D. J. Jones, Handbook of viscoelastic damping. *John Wiley & Sons, Inc.*, New York, 2001.

[17] L. J. Rayleigh, The Theory of Sound. *Dover*, New York, 1945.

[18] B. Mace, D. Duhamel, M. Brennan, L. Hinke. Finite element prediction of wave motion in structural waveguides. *Journal of the Acoustical Socitey of America*, **117**, 2835-2843, 2005.

[19] L. Brillouin, Wave propagation in periodic structures. *Dover*, New York, 1953.

[20] J. M. Renno, B. R. Mace, Calculating the forced response of two-dimensional homogeneous media using the wave and finite element method. *Journal of Sound and Vibration*. **329**, 5474-5488, 2010.

[21] J. M. Renno, B. R. Mace. Calculating the forced response of two-dimensional homogeneous media using the wave and finite element method. *Journal of Sound and Vibration*. **330**, 5913-5927, 2011.

[22] E. J. Hinch, Perturbation Methods. *Cambridge University Press*, 1991.